Geophysical Research Letters

Supporting Information for

Disruption of drought teleconnections between ENSO-influenced regions around 1700 CE

M.C.A. Torbenson[1], D.W. Stahle[2], E.R. Cook[3], B.I. Cook[3,4], U. Büntgen[5,6,7], F. Chen[8,9], E. Tejedor[10], J.H. Stagge[11], M. Trnka[6,12], D.J. Burnette[13], W. Yue[8], & J. Esper[1,6]

1 Department of Geography, Johannes Gutenberg University, Mainz, Germany.

2 Department of Geosciences, University of Arkansas, Fayetteville, United States.

3 Lamont-Doherty Earth Observatory, Columbia University, New York, United States.

4 NASA Goddard Institute for Space Studies, New York, United States.

5 Department of Geography, University of Cambridge, Cambridge, United Kingdom.

6 Global Change Research Institute, Czech Academy of Sciences, Brno, Czech Republic.

7 Department of Geography, Faculty of Science, Masaryk University, Brno, Czech Republic.

8 Institute of International Rivers and Eco-Security, Yunnan University, Kunming, China.

9 Institute of Desert Meteorology, Chinese Meteorological Administration, Urumqi, China.

10 Department of Geology, National Museum of Natural Sciences – Spanish Research Council, Madrid, Spain.

11 Department of Civil, Environmental and Geodetic Engineering, Ohio State University, Columbus, United States.

12 Department of Agrosystems and Bioclimatology, Mendel University in Brno, Brno, Czech Republic.

13 Department of Earth Sciences, University of Memphis, Memphis, United States.

Contents of this file

SUPPLEMENTARY TABLES AND FIGURES

Supplementary Table 1. Loadings of principal components (PC) 1-4 for the period 1600-2005 and 1600-2000 for the drought atlas and PHYDA regional PDSI estimates, respectively. The values on the bottom row represent the correlation between instrumental eMEI and the PCs for 1871-2005/2000.

	Drought atlases				PHYDA			
	PC1	**PC2**	**PC3**	**PC4**	**PC1**	**PC2**	**PC3**	**PC4**
iEU	0.75	0.63	0.17	-0.03	0.94	-0.31	0.14	0.04
SeA	-0.56	0.01	0.66	-0.50	-0.64	-0.03	0.19	0.75
EA	-0.54	0.21	0.48	0.66	-0.64	-0.14	0.75	-0.11
TxMx	0.72	-0.64	0.28	0.08	0.63	0.75	0.21	0.03
eMEI	0.72	-0.11	-0.20	0.01	0.62	0.11	0.05	-0.34

Supplementary Table 2. Dates of the ten tropical volcanic events considered in the analysis, with estimated volcanic stratospheric sulfur injections (VSSI) in Tg sulfur (Toohey & Sigl 2017). Model number and corresponding year of lowest inter-regional correlation in the CESM-LME runs are also given.

Year CE	VSSI	CESM-LME # (year)
1108	19.1	9 (1111)
1171	18.0	
1230	23.8	7 (1246)
1257	59.4	
1345	15.1	
1458	32.9	2 (1466)
1600	18.9	8 (1618)
1640	18.6	4 & 6 (1657 & 1652)
1695	15.7	
1815	28.0	

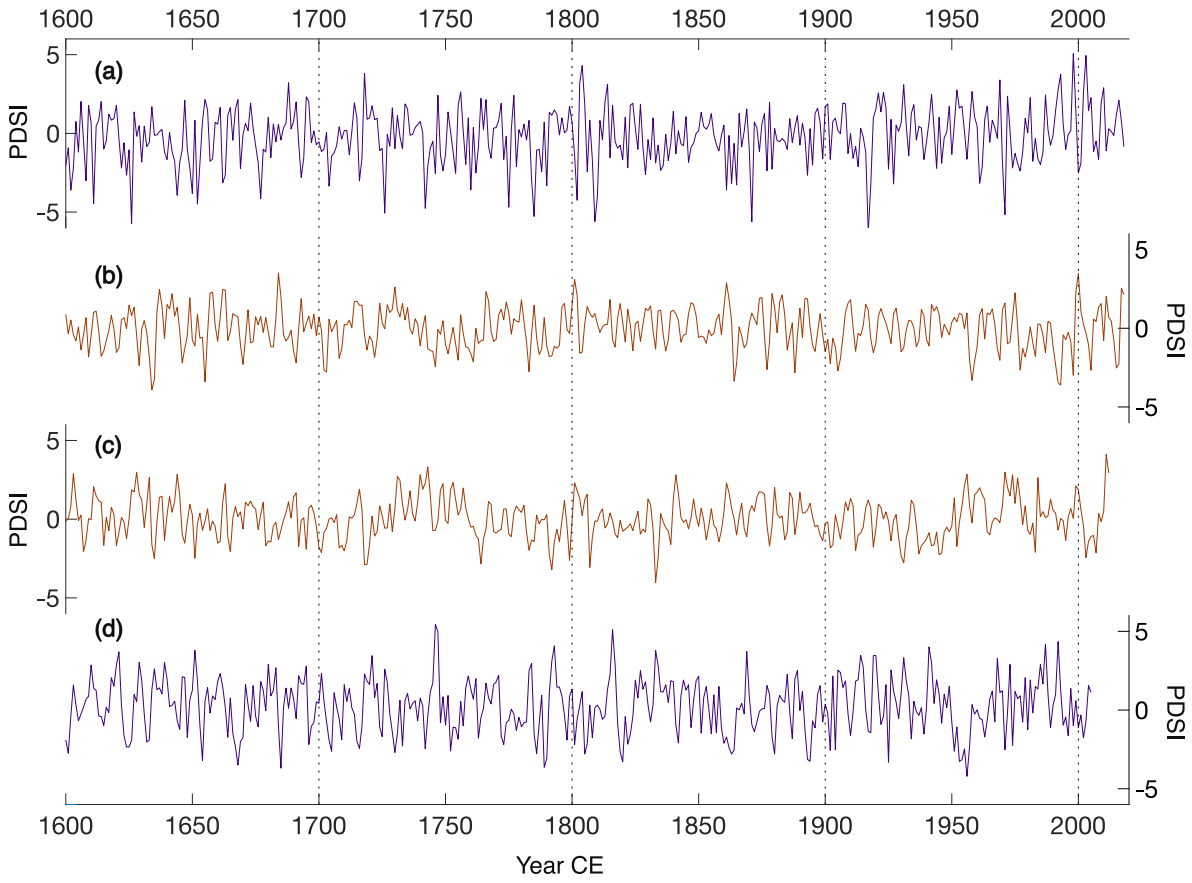

Supplementary Figure 1. Reconstructed PDSI from the drought atlases used in the analysis, starting in 1600 CE: (a) Inner Eurasia (iEU); (b) Southeast Asia (SeA); (c) Eastern Australia (EA); and (d) the Tex-Mex region of southwestern North America (TxMx).

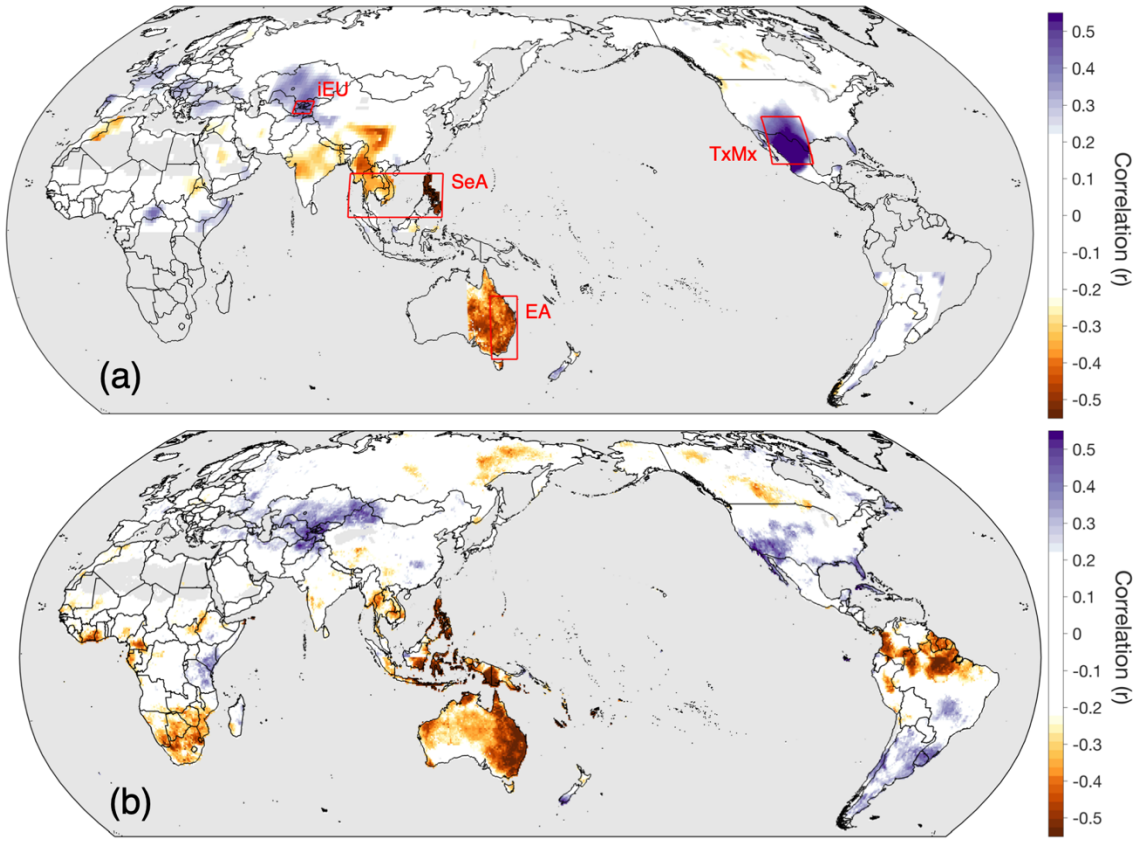

Supplementary Figure 2. (a) As Figure 1a but for the period 1871-1978. (b) Correlations between DJFM extended MEI and instrumental scPDSI for the period 1950-2005. Grey color on land indicates space without CRU data coverage. All correlations for the Northern Hemisphere are calculated with JJA scPDSI and with DJF scPDSI for the Southern Hemisphere (to align with the targets of the drought atlases).

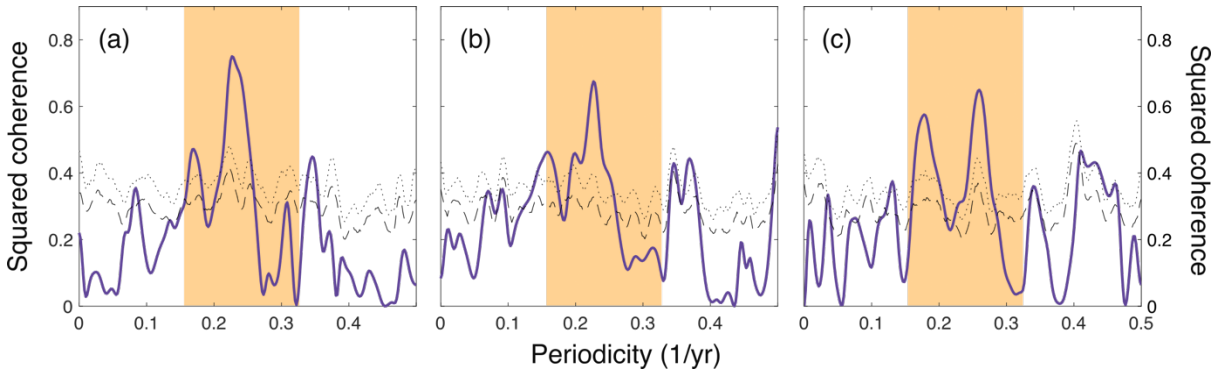

Supplementary Figure 3. Spectral agreement between the regional Southeast Asia PDSI reconstruction and the reconstructions for: (a) inner Eurasia; (b) Eastern Australia; and (c) TexMex are plotted (purple lines) for the longest possible overlap. Dotted (dashed) lines represent the 5th (10th) percentile confidence interval. The generalized ENSO band of 3-7 years is highlighted in yellow.

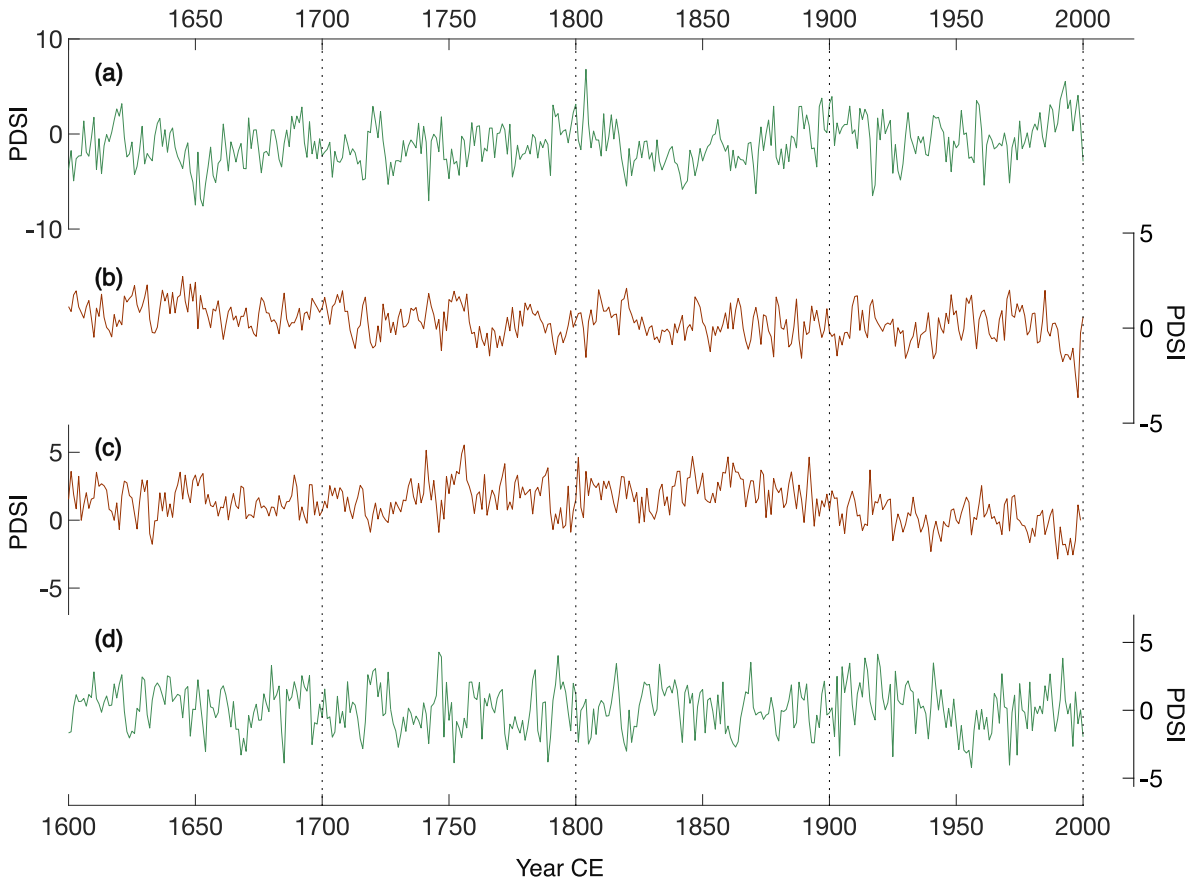

Supplementary Figure 4. PDSI estimates from the PHYDA v2 (Steiger et al. 2018), starting in 1600 CE: (a) Inner Eurasia (iEU); (b) Southeast Asia (SeA); (c) Eastern Australia (EA); and (d) the Tex-Mex region of southwestern North America (TxMx). Note the different y-axis.

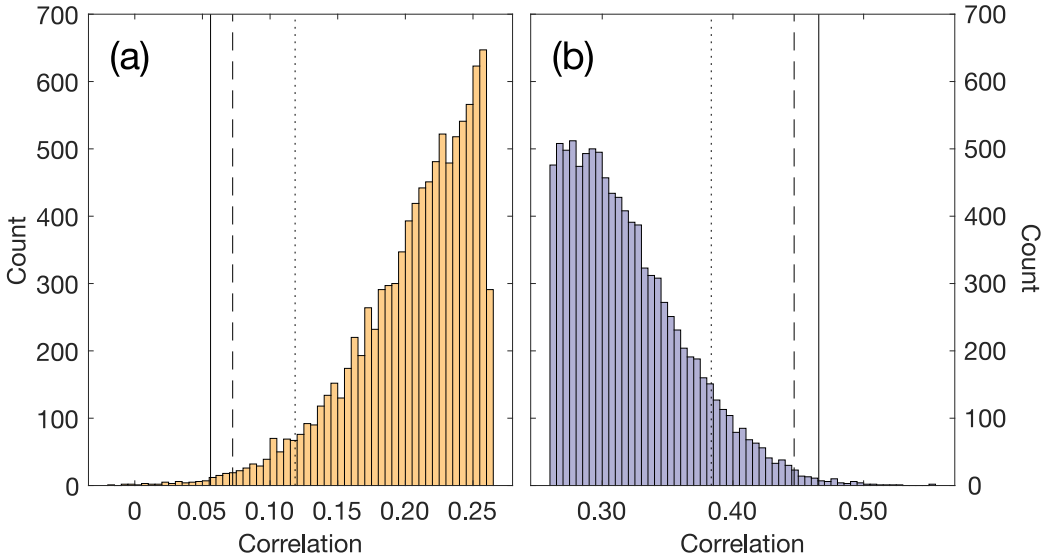

Supplementary Figure 5. Distributions of (a) minimum and (b) maximum averaged correlation values from a 10,000-run Monte Carlo simulation using the phase-scrambling approach. Lines indicate the 5 (dotted), 1 (dashed), and 0.5 (solid) percentiles of respective distribution.

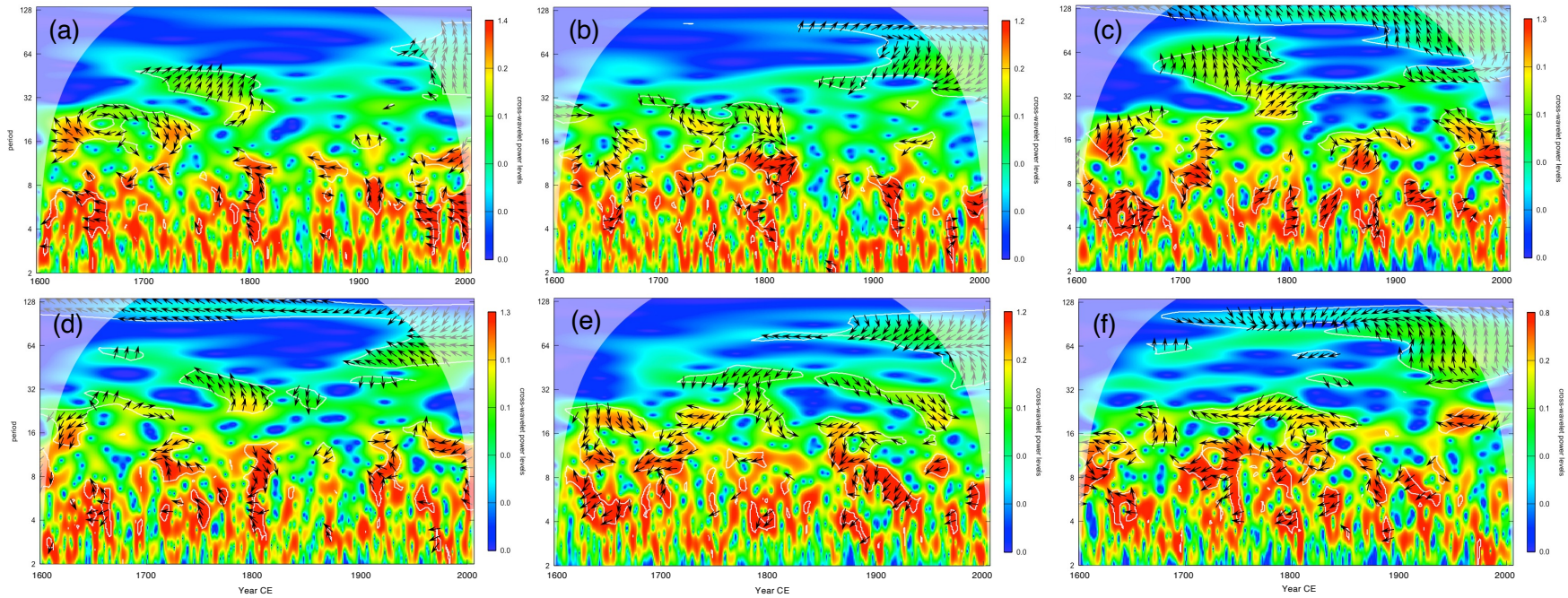

Supplementary Figure 6. Wavelet coherence plots for each of the four regional pairs (panels correspond to the pairs of Figure 2). Black arrows indicate significance ($p < 0.05$), with a direction to the right representing in-phase and left out-of-phase.

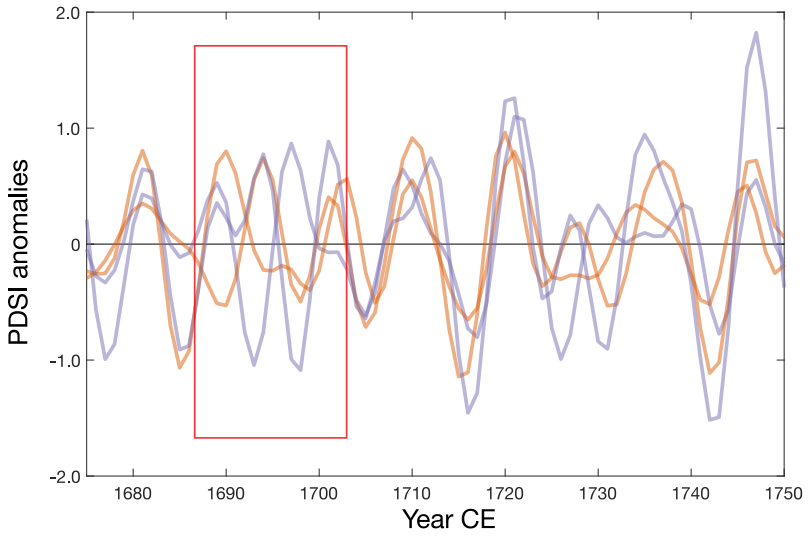

Supplementary Figure 7. The 3-7 year waveforms from the four regional PDSI reconstructions; purple colors indicating iEU and TxMx, orange colors SeA and EA. The orange lines have been inverted. The red box highlights a period of out-of-phase behavior between the waveforms.

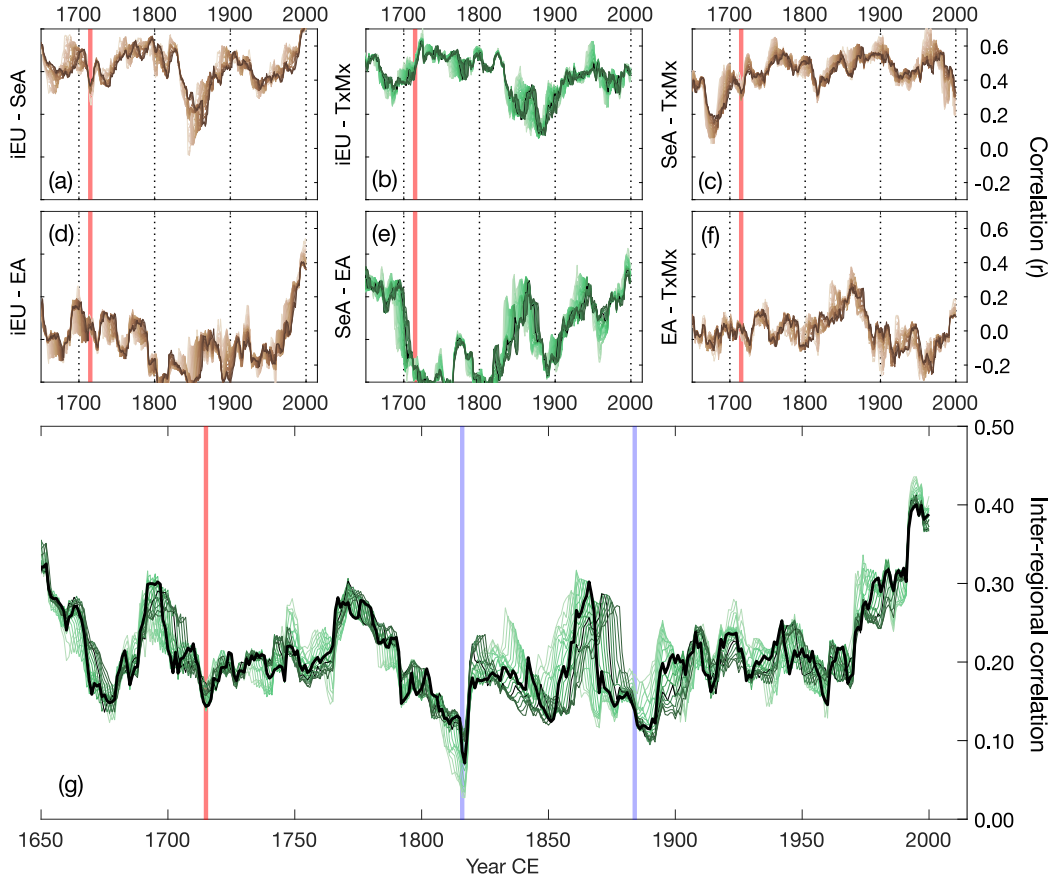

Supplementary Figure 8. (a-f) Same as for Figure 2 but for regional PDSI estimates from the PHYDA (Steiger et al. 2018). Green colors indicate positive correlations, brown colors negative. (g) Sign-adjusted inter-series correlation between regional PDSI estimates for 40-to-60-year running windows, with the 50-year window highlighted in black.

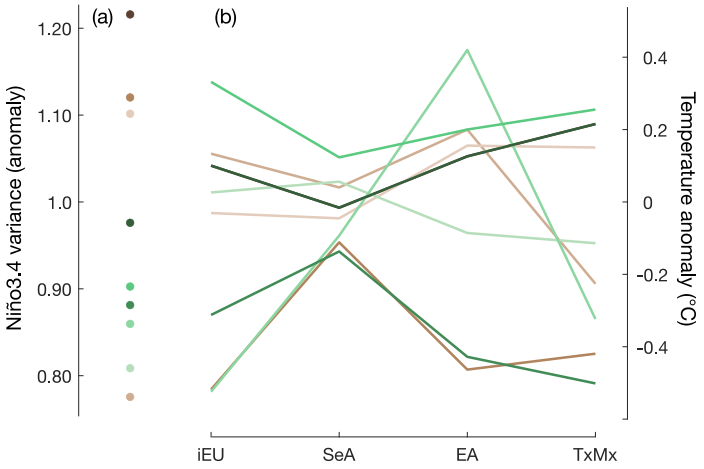

Supplementary Figure 9. (a) variance anomaly of the Niño3.4 index for the 50-year period leading up to the lowest point of inter-regional correlation in the nine tested CESM-LME members. (b) Temperature anomalies for the same season as the PDSI estimates (JJA/DJF) for the 50-year period leading up to the lowest point. Colors correspond to Figure 3.